Journal of Medicinal Chemistry

ARTICLE

pubs.acs.org/jmc

Exploring the Size Limit of Templates for Inhibitors of the M2 Ion Channel of Influenza A Virus

María D. Duque,[†] Chunlong Ma,[‡,#] Eva Torres,[†] Jun Wang,[§] Lieve Naesens,[∥] Jordi Juárez-Jiménez,[⊥] Pelayo Camps,[†] F. Javier Luque,[⊥] William F. DeGrado,[§] Robert A. Lamb,[#,∞] Lawrence H. Pinto,[‡] and Santiago Vázquez*[,†]

[†]Laboratori de Química Farmacèutica (Unitat Associada al CSIC), Facultat de Farmàcia, and Institute of Biomedicine (IBUB), Universitat de Barcelona, Av. Diagonal 643, Barcelona E-08028, Spain

[‡]Department of Neurobiology and Physiology, Northwestern University, Evanston, Illinois 60208-3500, United States

[§]Department of Chemistry and Department of Biochemistry and Biophysics, School of Medicine, University of Pennsylvania, Philadelphia, Pennsylvania 19104-6059, United States

[∥]Rega Institute for Medical Research, Katholieke Universiteit Leuven, 3000 Leuven, Belgium

[⊥]Departament de Fisicoquímica, Facultat de Farmàcia, and Institut de Biomedicina (IBUB), Universitat de Barcelona, Av. Diagonal 643, E-08028, Barcelona, Spain

[#]Department of Molecular Biosciences, Northwestern University, Evanston, Illinois 60208-3500, United States

[∞]Howard Hughes Medical Institute, Northwestern University, Evanston, Illinois 60208-3500, United States

Supporting Information

ABSTRACT: Amantadine inhibits the M2 proton channel of influenza A virus, yet its clinical use has been limited by the rapid emergence of amantadine-resistant virus strains. We have synthesized and characterized a series of polycyclic compounds designed as ring-contracted or ring-expanded analogues of amantadine. Inhibition of the wild-type (wt) M2 channel and the A/M2-S31N and A/M2-V27A mutant ion channels were measured in *Xenopus* oocytes using two-electrode voltage clamp (TEV) assays. Several bisnoradamantane and noradamantane derivatives inhibited the wt ion channel. The compounds bind to a primary site delineated by Val27, Ala30, and Ser31, though ring expansion restricts the positioning in the binding site. Only the smallest analogue **8** was found to inhibit the S31N mutant ion channel. The structure−activity relationship obtained by TEV assay was confirmed by plaque reduction assays with A/H3N2 influenza virus carrying wt M2 protein.

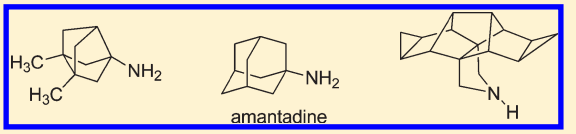

INTRODUCTION

The M2 protein of the influenza A virus forms a pH-gated proton channel that is essential for virus replication.[1,2] The influenza virus enters its target cells by receptor-mediated endocytosis, which is followed by acid-induced fusion of the viral and endosomal membranes. This fusion event is mediated by a conformational change of the influenza hemagglutinin proteins, triggered by the low pH in the endosome lumen.[3] The endosomal pH also activates the membrane-spanning A/M2 protein, which acts as a proton channel to conduct protons into the virion interior. As a result of decreased intravirion pH, the viral ribonucleoprotein is uncoated and transferred, after viral fusion with the endosome, to the cytoplasm.[4] In addition, it has been shown that for some influenza strains the A/M2 proton channel function is required for preventing a premature hemagglutinin conformation transition when newly synthesized viral proteins are trafficked through the trans-Golgi network.[5]

The highly conserved $H_{37}xxxW_{41}$ motif in the transmembrane (TM) domain of the A/M2 protein is responsible for its channel activity and proton selectivity.[6,7] The channel function of wt A/M2 is efficiently inhibited by two FDA approved drugs, amantadine (Amt) and rimantadine, as well as by a few new compounds such as **1** (BL-1743) and its analogues **2** and **3** (Chart 1).[8−10] Naturally arising single amino acid substitutions associated with Amt resistance, such as L26F, V27A, A30T, S31N, and G34E, are all located outside the $H_{37}xxxW_{41}$ motif.[11−14] Extensive studies suggest that these residues contribute to delineate the binding pocket for the inhibitors,[15−21] although Schnell and Chou showed that rimantadine can also bind to Asp44 of M2 TM in detergent solutions; this residue is found at the external lipid-facing helix interface, and this finding has been taken to imply an allosteric mechanism.[22] Even though the precise nature of the binding site of the inhibitors has been the subject of an intense debate, a series of functional evidence supports the binding to the interior of the channel. (1) A chimeric channel comprising A/M2 residues 24−36 embedded in an Amt-insensitive channel shows 85% inhibition by Amt.[23] (2) Amt and the known pore-residing inhibitor **1** compete for inhibition of the channel.[24] (3) Mutation of Asp44 to each of

Received: October 15, 2010
Published: April 05, 2011

seven amino acids does not reduce Amt inhibition.[18,25] Recently, a solid state (ss) NMR study and,[15] independently, a series of surface plasmon resonance experiments[26] showed that the external lipid-facing Asp44 site has much lower affinity than the lumenal site. These results suggest that drug binding within the pore is pharmacologically relevant.

Amt-resistant mutants are frequently detected among the two currently circulating subtypes of influenza A virus, A/H3N2 and A/H1N1, with the S31N mutation being observed in more than 90% of influenza A isolates in certain years.[27,28] More recently, the pandemic H1N1 swine flu virus, which is Amt resistant, was the cause of global and significant morbidity and mortality.[29,30] Thus, there is an urgent need for the development of novel anti-influenza drugs that are effective against the most common Amt-resistant mutants.[27,28]

This study reports novel scaffolds designed to bind to the high affinity site of the A/M2 channel. We have found that the wt channel can be inhibited by several polycyclic compounds covering a priori an unexpectedly large diversity in size. We have identified a promising compound, **8**, that is capable of inhibiting the M2-S31N mutant ion channel.

CHEMISTRY

Although Amt and rimantadine are well-known antiviral drugs and their structure−activity relationships have been previously examined,[8,31−50] quite surprisingly few ring-contracted or ring-expanded analogues have been synthesized.[32] Moreover, little effort has been paid to investigate the influence of polycyclic scaffolds on the inhibitory activity,[33,51−56] the guanidine **1** and related spiro-piperidine compounds being a notable exception (Chart 1).[9,10,24] Recently, we have described the synthesis and characterization of ring-contracted analogues of Amt and rimantadine, such as noramantadine derivatives **4**−**7** and bisnor-adamantane derivatives **8** and **9**.[57] We have also synthesized 2-oxa-analogues of Amt, such as **10** and **11** (Chart 2).[58] We tested these compounds against the influenza A/H1N1 and A/H3N2 subtypes in Madin−Darby canine kidney (MDCK) cells and found that primary amine **4** showed reasonable antiviral activity.

Chart 1. Structures of Amantadine, Rimantadine, 1 (BL-1743), 2 (3-Azaspiro[5,5]undecane), and 3 (Spiro[5.5]undecan-3-amine)

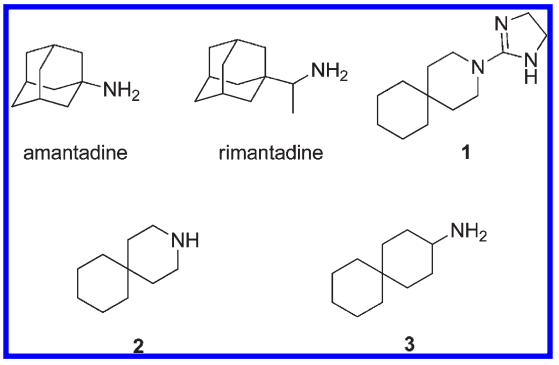

To further explore the impact of the polycyclic ring size on the inhibition of the A/M2 channel, we have now synthesized larger analogues of Amt using pentacyclic and hexacyclic scaffolds. The pentacyclo[6.4.0.0^{2,10}.0^{3,7}.0^{4,9}]dodecane scaffold has been used in the synthesis of polycyclic compounds of theoretical interest, such as dodecahedrane.[59] To the best of our knowledge, nevertheless, it has never been applied to the synthesis of compounds with potential biological interest. Starting from the diacid **12**,[60,61] we synthesized monoacid **13**, using a high-yielding synthetic sequence previously described by our group.[62] Schmidt reaction of acid **13** led to pentacyclic amine **14** in 82% yield. On the other hand, reaction of acid **13** with $SOCl_2$ followed by reaction of the acyl chloride with NH_4OH led to amide **17** that was reduced with $LiAlH_4$ to primary amine **18** (Scheme 1).

In order to explore the effect of the alkylation on the biological activity, **14** was treated with acetaldehyde and $NaCNBH_3$ to obtain tertiary amine **15** in 78% yield, while treatment of **18** with ethyl chloroformiate followed by reduction with $LiAlH_4$ led to secondary amine **19** in 41% overall yield. In order to study the effect of the basicity of the nitrogen atom on the inhibitory activity, we synthesized acetamidine **16** by reaction of amine **14** with methyl acetimidate. Unfortunately, several attempts to synthesize the corresponding guanidine were unsuccessful (Scheme 1).

The synthesis of the conformationally more rigid pyrrolidine-based derivatives **21**, **22**, and **24** started from the reaction of diacid **12** with urea at 180 °C for 30 min to yield imide **20**, which was subsequently reduced with $LiAlH_4$ to give secondary amine **21** in 36% overall yield. Catalytic hydrogenation of **21** quantitatively furnished amine **22**. Besides, cyclopropanation of the two C=C bonds of **20** led to imide **23** that was reduced with $LiAlH_4$ to give amine **24** in 61% overall yield (Scheme 2).

All the new amines **14**, **15**, **18**, **19**, **21**, **22** and **24** and acetamidine **16** were fully characterized as hydrochlorides through their spectroscopic data and elemental analyses.

PHARMACOLOGICAL ACTIVITY AND STRUCTURE−ACTIVITY RELATIONSHIPS

Inhibition of wt and Amantadine-Insensitive A/M2 Ion Channels. The inhibitory activity of the compounds was tested on A/M2 channels expressed in *Xenopus* oocytes using the TEV

Chart 2. Structures of Ring-Contracted and Oxa Analogues of Amantadine

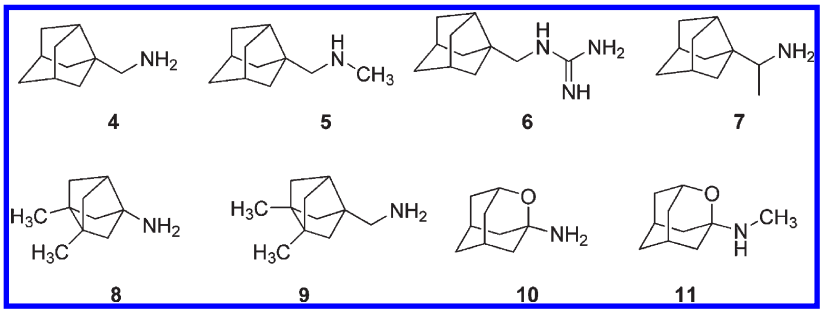

dx.doi.org/10.1021/jm101334y |*J. Med. Chem.* 2011, 54, 2646–2657

Scheme 1. Synthesis of New Amantadine Analogues with the Pentacyclo[6.4.0.0^{2,10}.0^{3,7}.0^{4,9}]dodecane Scaffold

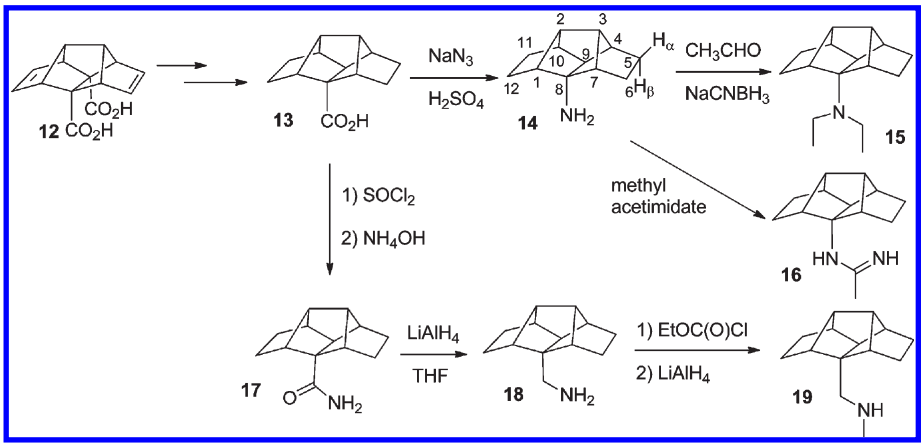

Scheme 2. Synthesis of Polycyclic Pyrrolidine Derivatives

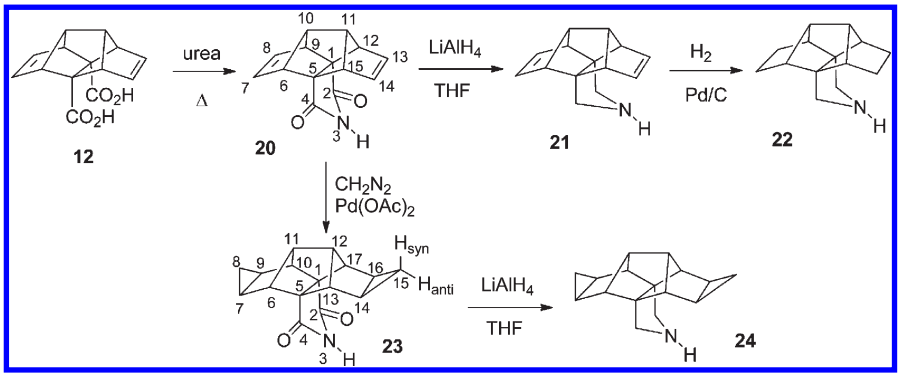

technique. All inhibitors were initially tested at 100 μM; those that inhibited the wt A/M2 channel activity by more than 80% were chosen for measurement of their IC$_{50}$. The results are given in Table 1 and Figure 1.

Amt inhibited wt A/M2 channel with an IC$_{50}$ of 16.0 μM in an isochronic (2 min) inhibition assay. Replacement of a methylene unit by an oxygen atom at position 2 of the adamantane ring (compounds **10** and **11**) led to a reduction in the inhibitory activity (IC$_{50}$ of 29.2 and 22.9 μM, respectively). Most strikingly, ring contraction of the Amt ring to noradamantane derivatives led to more active compounds. Thus, primary amine **4** showed an IC$_{50}$ of 7.1 μM, while guanidine **6**, with an IC$_{50}$ of 2.4 μM, was almost an order of magnitude more potent than Amt. The racemic rimantadine analogue **7** showed an IC$_{50}$ of 12.7 μM. Kolocouris et al. have previously found that in several adamantane derivatives, alkylation of the amine group caused a reduction of anti-influenza A virus activity.[40,43−47] This trend was also observed in going from compound **4** to its monomethylated derivative **5** (IC$_{50}$ of 17.1 μM). For this reason, no additional alkylated compounds were considered.

A second ring contraction led to bisnoradamantane derivatives, such as **8** and **9**. These smaller compounds behaved in a similar way as the bigger analogues. Thus, **8** showed an IC$_{50}$ of 17.0 μM, similar to that of Amt, while **9** showed an IC$_{50}$ of 7.2 μM, which is comparable with the inhibitory activity of **4**. Taken together, these results suggest that the A/M2 channel can be inhibited by compounds smaller than Amt. This observation is important, as most of the structure−activity relationships previously carried out on Amt analogues have concentrated on adamantane-substituted compounds with overall larger structures than Amt. Among all the new compounds tested, **8** was the only one able to inhibit A/M2 S31N channel with an IC$_{50}$ of 252 μM, slightly higher than that of Amt (IC$_{50}$ = 200 μM). Also, at 100 μM, **8** inhibited the A/M2 V27A channel activity by 10.6%, quite similar to Amt (10.8%).

Taking into account that the bisnoradamantane derivative **8** showed an interesting activity against wt and S31N A/M2 channels, compounds **14**, **15**, **16**, **18**, and **19** were synthesized. While being derivatives of the pentacyclo[6.4.0.0^{2,10}.0^{3,7}.0^{4,9}]-dodecane, a larger polycyclic scaffold, their structures also contain a bisnoradamantane subunit. Unfortunately, they performed poorly in the M2 inhibition experiments, with the diethylated derivative **15** being, not surprisingly, the least active compound in this series.

It has been suggested that in designing Amt analogues, pyrrolidine or piperidine derivatives may result in a more favorable orientation inside the M2 channel pore compared to freely rotating alkylamine chains.[48] Thus, we tested conformationally more rigid amines **21**, **22**, and **24**. In sharp contrast with the pentacyclic derivatives from Scheme 1, diene **21** was shown to be able to inhibit wt A/M2 channel by more than 80%, showing an IC$_{50}$ of 33.5 μM. While hydrogenation of the two C=C double bonds led to a much less potent compound, bis-cyclopropanation slightly increased the potency, derivative **24** showing an IC$_{50}$ of

Table 1. Inhibitory Effect of the Synthesized Compounds on A/M2 wt, S31N, and V27A Proton Channels Functions[a]

	A/M2 wt (mean ± SE)		A/M2 S31N (mean ± SE)		A/M2 V27A (mean ± SE)	
compd	inhibition by 100 μM for 2 min (%)	IC_{50} (μM)	inhibition by 100 μM for 2 min (%)	IC_{50} (μM)	inhibition by 100 μM for 2 min (%)	IC_{50} (μM)
amantadine	91.0 ± 2.1	16.0 ± 1.2	35.6 ± 1.5	199.9 ± 13.5	10.8 ± 2.0	ND
4	97.1 ± 0.1	7.1 ± 0.4	0	ND	0	ND
5	92.2 ± 1.2	17.1 ± 1.3	0	ND	0	ND
6	97.2 ± 0.7	2.4 ± 0.1	0	ND	0	ND
7	93.2 ± 1.0	12.7 ± 0.9	0	ND	0	ND
8	93.6 ± 0.9	17.0 ± 1.0	22.1 ± 0.2	252.2 ± 13.2	10.6 ± 0.7	ND
9	97.3 ± 0.4	7.2 ± 0.3	0	ND	17.6 ± 1.8	ND
10	88.2 ± 0.3	29.2 ± 1.2	0	ND	0	ND
11	91.7 ± 0.7	22.9 ± 1.4	0	ND	0	ND
14	4.8 ± 2.8	ND	0	ND	0	ND
15	0	ND	0	ND	0	ND
16	9.3 ± 2.4	ND	0	ND	2.2 ± 1.3	ND
18	12.8 ± 1.0	ND	0	ND	0	ND
19	14.7 ± 1.8	ND	0	ND	5.0 ± 2.2	ND
21	82.5 ± 0.8	33.5 ± 1.6	0	ND	9.2 ± 1.0	ND
22	39.7 ± 1.0	ND	0	ND	14.8 ± 0.5	ND
24	86.5 ± 0.8	24.0 ± 2.1	0	ND	17.7 ± 0.5	ND

[a] ND, not determined. Isochronic (2 min) values for IC_{50} are given. K_d was obtained for selected compounds by global fitting of circular dichroism (CD) data of ligand titration to wt A/M2TM (22−46) using Igor Pro (wavemetrics). See text and Supporting Information for details. K_d values are as follows: amantadine, 3.9 μM; **8**, 4.7 μM; **10**, 91.6 μM; **21**, 74.9 μM; **24**, 231.5 μM.

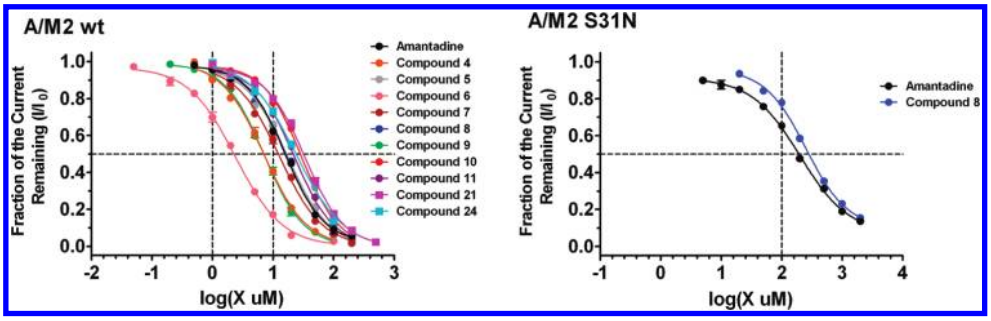

Figure 1. Dose-response curves on A/M2 wt and A/M2 S31N proton channels. Isochronic inhibition curves were generated for selected compounds that caused, in initial inhibition experiments with one compound concentration of 100 μM, more than 80% inhibition of A/M2 wt channel activity and more than 20% of S31N mutant proton channel activity. The inhibition efficacy of the compounds was assessed by comparing the residual membrane current (I) after 2 min of application of the compound to the maximum membrane current (I_0) before the application of the compound at pH 5.5. For each compound, seven to nine concentrations were used, and three oocytes were used at each concentration. The dose-response relationship was applied to the results by Origin 6 software, and best fit IC_{50} values are listed in Table 1.

24.0 μM. Interestingly, **24** (at 100 μM) inhibited the A/M2 V27A channel activity by 17.7%, which is superior to Amt (10.8%), although much less than **3** (53.4%).[24]

Molecular Modeling. To examine the effect of ring expansion on the binding to the A/M2 ion channel, we performed computational studies with **24**. Prior to studying the binding of **24**, however, we performed combined docking calculations and restrained molecular dynamics (MD) using the experimental data available for Amt. Previous X-ray[20] and ssNMR[15] studies have suggested that Amt mainly binds to the region of the channel comprising residues Val27 and Ser31 and that the amino group is oriented toward the C-terminal end of the pore. Our modeling studies, undertaken with an initial orientation of Amt in which the amino group was directed toward the C-terminus, agreed with this binding mode, as seen in snapshots sampled in a 40 ns restrained MD simulation (Figure 2, top left). The axis of Amt deviated ~7° from the pore axis, and the center of the cage deviated ~0.3 Å from the plane defined by the four Ser31 C_α atoms (see Figure S1 in Supporting Information). These findings agree with the structural features derived from ssNMR data (tilt angle of ~13° and height from the Ser31 C_α plane close to 0 Å[15]) and with the binding mode of Amt found in MD simulations of the channel at low pH conditions.[63] Remarkably, three water molecules were on average hydrogen-bonded to the amino group along the trajectory, thus enabling the formation of contacts with the dense network of water molecules surrounding the His37 box.[64]

Docking computations led to an alternative binding mode for Amt in which the amino group was hydrogen-bonded to both the hydroxyl group of Ser31 and the carbonyl group of Val27 of the

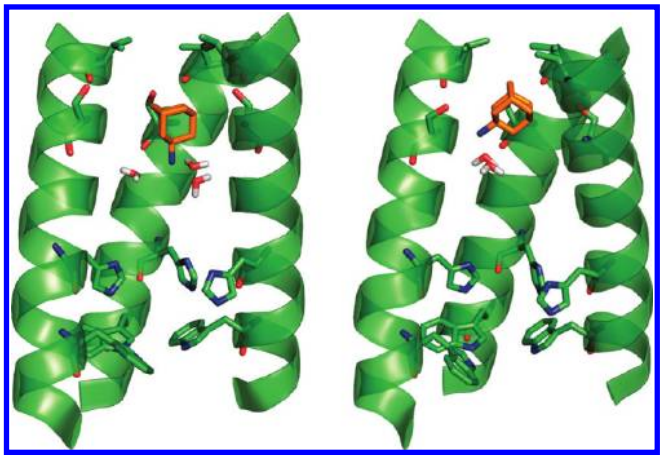

Figure 2. Structural models of putative binding modes of amantadine (orange) in the A/M2 ion channel suggested to account for the major (left) and minor (right) fractions identified by NMR data for amantadine bound to the channel.[15] Residues Val27, Ser31, His37, and Trp41 are shown in stick. For the sake of clarity, one transmembrane helix is not shown.

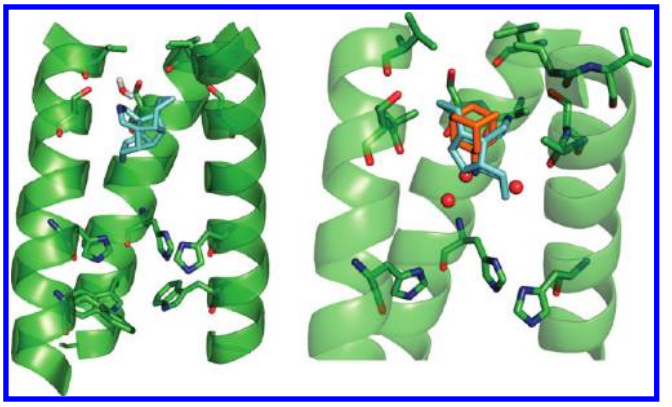

Figure 3. (Left) Structural model of the putative binding mode of compound **24** (blue) in the A/M2 ion channel (residues Val27, Ser31, His37, and Trp41 are shown in stick). (Right) Superposition of the binding modes of Amt and **24** (residues Val27, Ala30, Ser31, and His37 are shown in stick; hydrating waters of the protonated amine of Amt are shown as red spheres). For the sake of clarity, one transmembrane helix is not shown.

same TM chain. By use of this alternative docked pose as a starting structure, a slight readjustment of Amt was observed at the beginning of the MD trajectory, leading to the loss of the hydrogen bond with Val27, even though the amino group retained its hydrogen bonding with the hydroxyl group of Ser31 (Figure 2, top right; see also Figure S2 in Supporting Information). Moreover, the amino group became hydrogen-bonded with up to two water molecules during the trajectory. Interestingly, the axis of Amt deviated around 52° from the pore axis, in agreement with the minor fraction of M2-bound Amt observed from ssNMR data, found to have a tilt angle of 54.7°.[15]

We also performed an MD simulation starting with Amt oriented along the axis but with its amino group pointing toward the N-terminus. In this case, both the tilt angle of Amt (~37°) and the deviation from the Ser31 C_α plane (1.2 Å) clearly differed from those of the ssNMR data. Solvent interaction energy (SIE) calculations were performed to check the interaction free energy of the three binding modes. The results (see Supporting Information) revealed that the interaction free energies differ by 0.9 kcal/mol, which is less than the error estimated for those calculations (around 1.3 kcal/mol). Under these circunstamces, the use of the structural parameters such as the tilt angle and the separation from the plane defined by Ser31 C_α atoms, which are directly derived from experimental NMR data, seems to be better suited to discriminate between the different binding modes of Amt. On the basis of these results, the two binding modes shown in Figure 2 are suggested to be representative of the major and minor fractions of the Amt-bound A/M2 ion channel.

The chemical nature of the skeleton of the ring-contracted compounds not only retains the amphiphilic nature of Amt but also has a moderate impact on the overall shape of the compounds. Thus, the van der Waals surface and volume of those compounds vary from 205 $Å^2$ and 147 $Å^3$ for **4** to 231 $Å^2$ and 162 $Å^3$ for **9**, which are comparable with values of 202 $Å^2$ and 146 $Å^3$, respectively, for Amt. Accordingly, such a chemical resemblance should enable the ring-contracted compounds to mimic the binding mode of Amt in the M2 channel, thus leading to small variations in the IC_{50} values (from 7.1 to 17.1 μM, which are comparable with the IC_{50} of 16 μM determined for Amt). At this point, it is worth noting that the replacement of one of the carbon atoms in β position in Amt by an oxygen atom has a larger effect on the inhibitory activity, as noted in the IC_{50} of 29.2 μM determined for the oxa analogue **10**. This effect can likely be attributed to two factors: (i) the lack of a suitable partner in the transmembrane helix that could interact with the lone pairs of the oxygen atom (see Figure S3 in Supporting Information) and (ii) a slightly worse fit of the region filled by Amt, as suggested by the smaller surface (189 $Å^2$) and volume (138 $Å^3$) of **10** compared to Amt.

In light of the preceding discussion, the similar inhibitory activity determined for Amt and the ring-expanded compound **24** (IC_{50} = 24.0 μM) is totally unexpected, as the chemical structure of this latter compound leads to the largest increase in the molecular size (by around 36%) relative to Amt (van der Waals surface and volume of 261 $Å^2$ and 198 $Å^3$ for **24**). It is worth noting that previous studies have already reported larger compounds with inhibitory activity at the A/M2 channel, as illustrated by compounds **1**−**3** in Chart 1. However, the expansion of the chemical skeleton took place along the molecular axis, which should increase the volume filled by the compound in the interior of the channel. In contrast, the ring-expansion strategy presented here occurs along the normal to the main axis, and it can be accomplished without a significant reduction in inhibitory potency even though such a chemical modification would prevent the ring-expanded compound from adopting a binding mode that mimics the arrangement of Amt in the channel. Thus, attempts to accommodate compound **24** in the same region occupied by Amt with the amino group toward the C-terminus failed because of severe steric clashes with the residues in the TM helices that surrounded the compound.

Docking calculations were then used in conjunction with MD simulations in order to explore the binding mode of compound **24**. Inspection of the docked poses indicated that **24** was able to bind the primary site through hydrogen bonds with Ser31 and Val27. Subsequent refinement by restrained MD simulations showed a slight readjustment of the binding mode, as **24** was found to retain the direct hydrogen bond to Ser31, but a water molecule was bridging the amino group and the carbonyl unit of Val27 in a neighboring TM chain (Figure 3, left). In addition, the

large size of the cage imposed a distinct positioning in the binding site to alleviate steric clashes in the interior of the channel, and the main axis of the fused ring deviated around 40° from the pore axis. In turn, this binding mode facilitated the formation of van der Waals contacts with the side chain of Ala30. To further check the binding mode proposed for **24**, two additional MD simulations were run by placing this compound in distinct starting orientations (see Molecular Modeling in Experimental Section and Figure S4 in Supporting Information). In both cases the arrangement of **24** at the end of the simulations mimicked the binding mode shown in Figure 2, as noted in the similarity of the compound found in the three independent trajectories (see Figure S5 in Supporting Information), thus giving support to the tentative binding mode of the ring-expanded derivative.

Overall, even though molecular modeling results are consistent with the region delineated by residues Val27, Ala30, and Ser31 being the major binding site of **24**, its binding is more constrained than that of Amt, leading to different arrangements of these compounds in the pore (Figure 3, right). Accordingly, we expect that the structure−activity relationships for ring-expanded analogues will differ considerably from those for Amt. In particular, it is worth noting the high asymmetry in the environment around the two cyclopropane rings of **24**. Thus, in one case the cyclopropane unit is oriented toward the hydrophobic ring formed by the four Val27. However, the other unit is embedded in the region filled by the hydrating water molecules placed around the protonated amine of Amt. Thus, even though a weak C−H···O hydrogen bond could be formed between the cyclopropane unit and the carbonyl group of Ala30, the disruption of the network of water interactions above the His ring can be expected to have a net destabilizing effect for the binding of **24**. Accordingly, it can be envisaged that breaking of the internal symmetry of **24** through the incorporation of polar groups in one of the cyclopropane units should facilitate the formation of favorable interactions with water molecules and therefore lead to an enhancement in the inhibitory activity.

Activity in Plaque Reduction Assays. The most potent compounds were tested for inhibition of influenza virus containing the wt A/M2 ion channel by plaque reduction assays (Figure 4). Plaque formation of wt influenza virus (strain A/Udorn/72) was strongly inhibited by Amt, **4**−**9**, and **24** at 5 μM compound concentrations, in agreement with electrophysiological recordings.

Binding of Selected Amines. We also assessed the binding of selected drugs to the TM domain of wt A/M2 protein (M2TM, residues 22−46), using a spectroscopic assay that relies upon changes in the CD spectrum of M2 induced by binding of drugs (Table 1 and Figure S6 in the Supporting Information). All drugs bound with a stoichiometry of approximately one drug per tetramer. At pH 7.4, bisnoradamantane amine **8** was found to bind to the tetrameric form of M2TM with low micromolar binding constant (K_d = 4.7 μM), being approximately equipotent with Amt (K_d = 3.9 μM).

Cytotoxicity Evaluation. All of the synthesized amines were evaluated for cytotoxicity in MDCK cells, using a formazan-based cell viability assay. The concentration producing 50% cytotoxicity (CC_{50}) was higher than 500 μM (the highest concentration tested) for Amt, **8**, **10**, **11**, **14**, **16**, and **21**. Low cytotoxicity was also observed for compounds **4**, **7**, **15**, and **19** (CC_{50} of 357, 256, 119, and 224 μM, respectively). Compounds **9** and **24** had intermediate toxicity, their CC_{50} values being 79 and 61, respectively. Finally, compounds **5**, **6**, and **18** displayed relatively high cytotoxicity, since their CC_{50} values were <19.4, 10.5, and 12.0 μM, respectively.

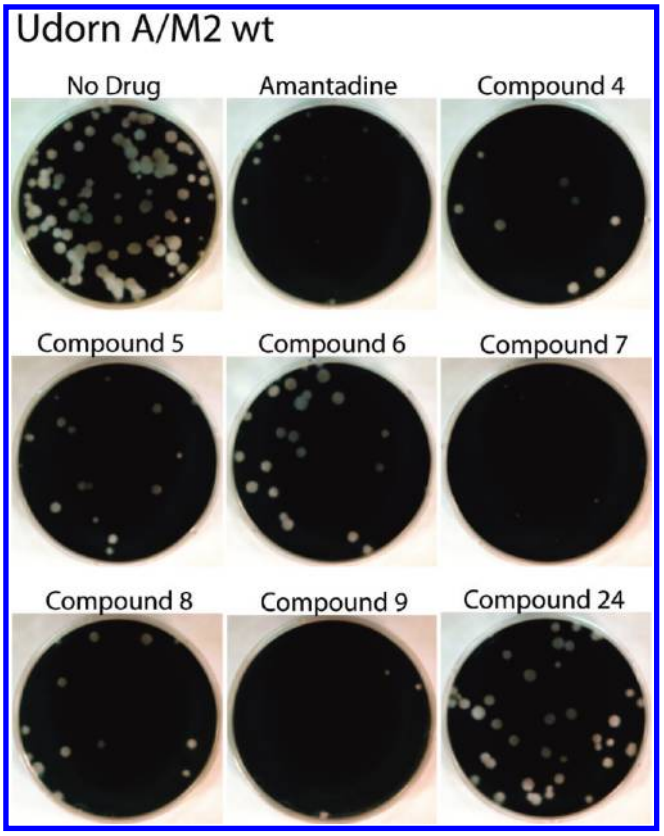

Figure 4. Plaque reduction assay with A/M2 wt influenza virus. The inhibitory effect of the compounds on influenza A virus replication was evaluated by plaque formation in MDCK cells in the presence or absence of the compounds (5 μM) as described in the Experimental Section. Plaque counts (number of plaques per well) are as follows: no drug, 78; amantadine, 10; **4**, 8; **5**, 14; **6**, 20; **7**, 6; **8**, 12; **9**, 3; **24**, 32.

CONCLUSIONS

The present work demonstrates that novel scaffolds exist for compounds that are capable of effective inhibition of the M2 ion channel of influenza A virus and can in fact inhibit the channel more effectively than amantadine. These scaffolds contain ring-expanded and ring-diminished variants of adamantine and are not inherently cytotoxic. The work confirms previous studies that found the binding site for adamantine to lie within the channel pore with the amino group directed toward the C-terminal of the helical bundle and suggests that ring-expanded compounds do not bind in a similar manner.

EXPERIMENTAL SECTION

Plasmid, mRNA Synthesis, and Microinjection of Oocytes. The cDNA encoding the influenza A/Udorn/72 (A/M2) was inserted into pGEM3 vector for the expression on oocyte plasma membrane. A/M2 S31N and A/M2 V27A mutants were generated by QuikChange site-directed mutagenesis kit (Agilent Technologies). The syntheses of mRNA and microinjection of oocytes have been described previously.[65]

Two-Electrode Voltage Clamp Analysis. Macroscopic membrane current was recorded 48−72 h after injection as described previously.[24] The tested compounds were applied at pH 5.5 at various concentrations

when the inward current reaches maximum. The compounds were applied for 2 min, and residual membrane current was compared with the membrane current before the application of compounds. Membrane currents were analyzed with pCLAMP 10.0 software package (Axon Instruments, Sunnyvale, CA).

Plaque Reduction Assay. Confluent monolayers of MDCK cells were incubated with serially diluted virus samples (A/Udorn/72) in DMEM with 1% bovine serum albumin (BSA) for 1 h at 37 °C. The inocula were removed, and the cells were washed with phosphate buffered saline (PBS). The cells were then overlaid with DMEM containing 1.2% Avicel microcrystalline cellulose (FMC BioPolymer, Philadelphia, PA) and *N*-acetyltrypsin (NAT, 1.0 μg/mL). To examine the effect of the compounds on plaque formation, MDCK cell monolayers were preincubated with DMEM supplemented with the compound (5 μM) at 37 °C for 30 min, and virus samples were preincubated with DMEM plus 1% BSA with the compound (5 μM) at 4 °C for 30 min before infection. At 2 days after infection, the monolayers were fixed and stained with naphthalene black dye solution (0.1% naphthalene black, 6% glacial acetic acid, 1.36% anhydrous sodium acetate).

Cytotoxicity Assays. The compound cytotoxicity was assessed as described.[66] Briefly, exponentially growing MDCK cells were grown in 96-well plates and test compounds were added in serial dilutions. After 72 h of incubation at 35 °C, cell viability was measured by the formazan-based MTS assay and the OD values were used to calculate the compounds concentrations causing 50% cytotoxicity (CC_{50}).

CD Titrations. CD titrations were conducted using materials and procedures described in a previous study.[24] Synthetic M2TM 22−46 (62.5 μM) was dissolved in DPC micelles (detergent concentration, 2.5 mM) potassium phosphate buffer (10 mM), pH 7.4. For titrations, the drug was added from concentrated solutions in the same buffer. Spectra were recorded in a 1 mm path length cuvette using a Jasco J-810 spectropolarimeter (Jasco, Easton, MD) at 25 °C with 1 nm step scans (4 s acquisitions, 3 accumulations). The ellipticity at 222 ± 1 nm was averaged to improve signal-to-noise and corrected for dilution factor.

Chemical Synthesis. General Methods. Melting points were determined in open capillary tubes with a MFB 595010 M Gallenkamp or a Büchi B-540 melting point apparatus. 300 MHz ^{1}H/75.4 MHz ^{13}C NMR spectra, 400 MHz ^{1}H/100.6 MHz ^{13}C NMR spectra, and 500 MHz ^{1}H NMR spectra were recorded on Varian Gemini 300, Varian Mercury 400, and Varian Inova 500 spectrometers, respectively. The chemical shifts are reported in ppm (δ scale) relative to internal tetramethylsilane, and coupling constants are reported in hertz (Hz). Assignments given for the NMR spectra of the new compounds have been carried out on the basis of DEPT, COSY ^{1}H/^{1}H (standard procedures), and COSY ^{1}H/^{13}C (gHSQC and gHMBC sequences) experiments. IR spectra were run on Perkin-Elmer Spectrum RX I or Thermo Nicolet Nexus spectrophotometers. Absorption values are expressed as wavenumbers (cm^{-1}); only significant absorption bands are given. Column chromatography was performed on silica gel 60 AC.C (35−70 mesh, SDS, ref 2000027). Thin-layer chromatography was performed with aluminum-backed sheets with silica gel 60 F_{254} (Merck, ref 1.05554), and spots were visualized with UV light and 1% aqueous solution of $KMnO_4$. The analytical samples of all of the new compounds which were subjected to pharmacological evaluation possessed a purity of ≥95% as evidenced by their elemental analyses.

(Pentacyclo[6.4.0.0^{2,10}.0^{3,7}.0^{4,9}]dodec-8-yl)amine Hydrochloride (14·HCl). To a solution of known acid **13** (2.50 g, 12.2 mmol) in CH_2Cl_2 (25 mL), concentrated H_2SO_4 (4 mL) was added. The mixture was heated to 50 °C. Then sodium azide (1.69 g, 26.0 mmol) was added portionwise and the heating was continued for 1.5 h. The mixture was cooled to 0 °C (ice−water bath). Ice (25 g) was added, and 2 N NaOH was added until basic pH was obtained. The two layers were separated, and the aqueous layer was extracted with EtOAc (4 × 20 mL). The combined organic extracts were dried with anhydrous Na_2SO_4, filtered, treated with excess of HCl in Et_2O, and concentrated in vacuo to give the hydrochloride of **14** (2.25 g, 82% yield). An analytical sample of **14**·HCl was obtained as a white solid by crystallization from methanol/Et_2O: mp >242 °C (dec); IR (KBr) ν 3200−2500 (max at 2948, 2926, 2882, and 2786, N−H, $^+$N−H, and C−H st) cm^{-1}; ^{1}H NMR (500 MHz, CD_3OD) δ 1.49 (s, 1 H, 9-H), 1.60−1.70 [complex signal, 6 H, 5(11)-H$_\alpha$, 5(11)-H$_\beta$ and 6(12)-H$_\alpha$], 1.71−1.79 [complex signal, 2 H, 6(12)-H$_\beta$], 2.32 [s, 2 H, 4(10)-H], 2.40 [s, 4 H, 1(7)-H and 2(3)-H]; ^{13}C NMR (100.6 MHz, CD_3OD) δ 21.9 [CH_2, C6(12)], 24.6 [CH_2, C5(11)], 48.6 [CH, C2(3)], 52.1 (CH, C9), 54.7 [CH, C4(10)], 56.3 [CH, C1(7)], 64.5 (C, C8). MS (EI), *m*/*e*: 175 ($M^{\cdot+}$, 17), 147 (100), 146 (19), 132 (16), 119 (32). Anal. Calcd for $C_{12}H_{17}N\cdot HCl\cdot 0.1H_2O$ (213.54): C 67.49, H 8.59, N 6.56. Found: C 67.49, H 8.68, N 6.56.

***N*,*N*-Diethyl(pentacyclo[6.4.0.0^{2,10}.0^{3,7}.0^{4,9}]dodec-8-yl)amine Hydrochloride (15·HCl).** To a solution of **14**·HCl (275 mg, 1.3 mmol) in MeOH (10 mL) were added $NaBH_3CN$ (95%, 172 mg, 2.6 mmol), acetic acid (0.4 mL), and acetaldehyde (0.22 mL, 3.9 mmol). The mixture was stirred for 4 h at room temperature. A second portion of $NaBH_3CN$ (95%, 86 mg, 1.3 mmol) and acetaldehyde (0.11 mL, 1.95 mmol) were added, and the mixture was stirred for an additional 18 h at room temperature. The mixture was concentrated in vacuo. Water (15 mL) was added, and the suspension was made basic with 2 N NaOH and extracted with EtOAc (4 × 10 mL). The combined organic extracts were washed with brine (2 × 25 mL), dried with anhydrous Na_2SO_4, filtered, treated with excess of HCl in Et_2O, and concentrated in vacuo to give the hydrochloride of **15** (269 mg, 78% yield). An analytical sample of **15**·HCl was obtained as a white solid by crystallization from MeOH/Et_2O: mp 206−207 °C; IR (KBr) ν 3100−2800 (max at 2956 and 2864, C−H st), 2700−2400 (max at 2624, 2549 and 2470, $^+$N−H st) cm^{-1}; ^{1}H NMR (500 MHz, CD_3OD) δ 1.45 [t, *J* = 7.5 Hz, 6 H, N-($CH_2\underline{CH_3}$)$_2$], 1.66−1.76 [complex signal, 6 H, 5(11)-H$_\beta$, 6(12)-H$_\alpha$ and 6(12)-H$_\beta$], 1.91−1.96 [complex signal, 3 H, 5(11)-H$_\alpha$ and 9-H], 2.39 [complex signal, 4 H, 2(3)-H and 4(10)-H], 2.72 [s, 2 H, 1(7)-H], 3.41−3.50 [complex signal, 4 H, N($\underline{CH_2}CH_3$)$_2$], 4.85 (s, NH); ^{13}C NMR (100.6 MHz, CD_3OD) δ 11.5 [CH_3, N($CH_2\underline{CH_3}$)$_2$], 23.8 [CH_3, C6(12)], 23.9 [CH_2, C5(11)], 48.2 [CH, C2(3)], 48.7 [CH_2, N($\underline{CH_2}CH_3$)$_2$], 51.5 (CH, C9), 54.3 [CH, 4(10)], 56.3 [CH, 1(7)], 79.4 (C, C8). MS (EI), *m*/*e* (%): 231 ($M^{\cdot+}$, 48), 216 (23), 203 (100), 202 (32), 188 (33), 175 (30), 136 (30). Anal. Calcd for $C_{16}H_{25}N\cdot HCl\cdot 0.15H_2O$ (270.54): C 71.03, H 9.80, N 5.18, Cl 13.10. Found: C 70.87, H 9.73, N 5.30, Cl 13.31.

***N*-(Pentacyclo[6.4.0.0^{2,10}.0^{3,7}.0^{4,9}]dodec-8-yl)acetamidine Hydrochloride (16·HCl).** A suspension of **14**·HCl (250 mg, 1.18 mmol), Et_3N (0.5 mL, 3.59 mmol) and methyl acetimidate hydrochloride (259 mg, 2.37 mmol) in THF (8 mL) was stirred at room temperature for 24 h. The precipitate was filtered and washed with THF and Et_2O. The filtrate was taken in H_2O (5 mL), and 5 N NaOH was added till basic pH was obtained. The suspension was stirred at room temperature for 1 h. The solid was filtered, washed with H_2O (3 × 5 mL), taken in EtOAc (10 mL), dried with anhydrous Na_2SO_4, filtered, treated with excess of HCl in Et_2O, and concentrated in vacuo to give the hydrochloride of **16** (124 mg, 42% yield) as a white solid. An analytical sample of **16**·HCl was obtained as a white solid by crystallization from EtOAc/Et_2O: mp >273 °C (dec); IR (KBr) ν 3500−2800 (max at 3368, 3135, 2940 and 2866, N−H, $^+$N−H and C−H st), 1670 and 1636 (C═N st) cm^{-1}; ^{1}H NMR (500 MHz, CD_3OD) δ 1.45−1.60 [complex signal, 4 H, 6(12)-H$_\alpha$ and 6(12)-H$_\beta$], 1.60−1.66 [complex signal, 5 H, 5(11)-H$_\alpha$, 5(11)-H$_\beta$ and 9-H], 2.27 [s, 2 H, 4(10)-H], 2.32 (s, 3 H, CH_3), 2.38 [broad s, 2 H, 2(3)-H], 2.87 [t, *J* = 3.5 Hz, 2 H, 1(7)-H], 7.62 (s, 1 H, NH), 9.16 (s, 1 H) and 9.34 (s, 1 H) (═NH_2^+); ^{13}C NMR (100.6 MHz, CD_3OD) δ 19.4 (CH_3, CH_3), 22.1 [CH_2, C6(12)], 25.1 [CH_2, C5(11)], 48.6 [CH, C2(3)], 52.8 [CH, C1(7)], 53.7 [CH, 4(10)], 55.4 (CH) and 55.5 (CH) (C9), 68.5 (C) y 68.6 (C) (C8), 166.0 [C, $CH_3(\underline{C}$═NH)NH]. MS (EI), *m*/*e* (%): 217 (23), 216 ($M^{\bullet+}$,

100), 201 (70), 199 (28), 198 (31), 188 (31), 160 (46), 159 (53), 147 (100), 146 (44), 137 (37), 132 (28), 130 (27), 129 (27), 119 (43), 109 (34), 91 (31), 80 (33), 77 (26), 59 (32). Anal. Calcd for $C_{14}H_{20}N_2 \cdot HCl \cdot 1.1H_2O$ (272.60): C 61.68, H 8.58, N 10.28, Cl 13.01. Found: C 61.52, H 8.76, N 10.22, Cl 13.44.

Pentacyclo[6.4.0.0^{2,10}.0^{3,7}.0^{4,9}]dodecane-8-carboxamide (17). A solution of acid **13** (1.00 g, 4.90 mmol) in $SOCl_2$ (20 mL, 0.27 mol) was heated under reflux for 2 h. The solution was concentrated in vacuo, taken in toluene (5 mL), and concentrated in vacuo (twice). A yellow oil, corresponding to the acyl chloride, was obtained. A solution of this oil in CH_2Cl_2 (5 mL) was cooled to 0 °C. NH_4OH (25% aqueous solution, 45 mL) was added dropwise, and the mixture was stirred at room temperature overnight. The mixture was extracted with CH_2Cl_2 (4 × 30 mL). The aqueous layer was acidified with concentrated HCl, extracted with ethyl acetate (3 × 30 mL), dried with anhydrous Na_2SO_4, filtered, and concentrated in vacuo to give starting acid **13** (40 mg). On the other hand, the organic phase of CH_2Cl_2 was washed with brine (2 × 30 mL), dried with anhydrous Na_2SO_4, filtered, and concentrated in vacuo to give the amide **17** (894 mg, 94% yield based in recovered starting material) as a white solid. An analytical sample of **17** was obtained by crystallization from CH_2Cl_2/hexane: mp 173−174 °C; IR (KBr) ν 3500−3150 (max at 3481, 3391, 3344, 3206, and 3187, N−H st), 300−2750 (max at 2973, 2943, 2908, and 2868 C−H st), 1651 (C═O st), 1607 (N−C═O st) cm^{-1}; ^{1}H NMR (500 MHz, $CDCl_3$) δ 1.45−1.67 [complex signal, 8 H, 5(11)-H$_\alpha$, 5(11)-H$_\beta$, 6(12)-H$_\alpha$ and 6(12)-H$_\beta$], 1.84 [t, J = 2.5 Hz, 1 H, 9-H], 2.23 [broad s, 2 H, 4(10)-H], 2.30 [m, 2 H, 2(3)-H], 2.39 [broad s, 2 H, 1(7)-H], 5.43 (broad signal, 1 H), and 5.96 (broad signal, 1 H) ($CONH_2$); ^{13}C NMR (100.6 MHz, $CDCl_3$) δ: 23.0 [CH_2, C6(12)], 24.1 [CH_2, C5(11)], 49.0 [CH, C2(3)], 50.0 (CH, C9), 53.5 [CH, C4(10)], 58.1 [CH, C1(7)], 59.4 (C, C8), 176.5 (C, CO). MS (EI), m/e (%): 204 (15), 203 ($M^{\bullet+}$, 100), 159 (57), 117 (28), 115 (21), 91 (34), 79 (21), 77 (24). Anal. Calcd for $C_{13}H_{17}NO$ (203.28): C 76.81, H 8.43, N 6.89. Found: C 76.76, H 8.52, N 6.85.

[(Pentacyclo[6.4.0.0^{2,10}.0^{3,7}.0^{4,9}]dodec-8-yl)methyl]amine Hydrochloride (18·HCl). To a stirred solution of amide **17** (598 mg, 2.94 mmol) in anhydrous THF (40 mL) at 0 °C, $LiAlH_4$ (375 mg, 95% purity, 9.40 mmol) was carefully added. When the addition was finished, the suspension was heated under reflux for 18 h. The mixture was cooled to 0 °C (ice−water bath), treated with 10 N NaOH (5 mL), and stirred at room temperature for 1 h. The obtained solid was filtered through Celite in vacuo and washed with CH_2Cl_2 (3 × 25 mL). The filtrate was dried with anhydrous Na_2SO_4, filtered, treated with excess of HCl in Et_2O, and concentrated in vacuo to give the hydrochloride of **18**. Crystallization from MeOH/Et_2O gave pure **18**·HCl as a white solid (396 mg, 60% yield): mp >255 °C (dec); IR (KBr) ν 3200−2700 (max at 2980, 2940 and 2861, N−H, $^+$N−H, and C−H st) cm^{-1}; ^{1}H NMR (500 MHz, CD_3OD) δ 1.14 [t, J = 2.5 Hz, 1 H, 9-H], 1.47−1.66 [complex signal, 8 H, 5(11)-H$_\alpha$, 5(11)-H$_\beta$, 6(12)-H$_\alpha$ and 6(12)-H$_\beta$], 2.20 [broad s, 4 H, 1(7)-H and 4(10)-H], 2.33 [m, 2 H, 2(3)-H], 3.11 (s, 2 H, CH_2NH$_2$), 4.86 (broad signal, 3 H, NH_3^+); ^{13}C NMR (100.6 MHz, CD_3OD) δ 23.1 [CH_2, C6(12)], 25.0 [CH_2, C5(11)], 38.5 (CH_2, CH_2NH_2), 49.2 [CH, C2(3)], 51.0 (C, C8), 53.0 (CH, C9), 53.7 [CH, C4(10)], 54.4 [CH, C1(7)]. MS (EI), m/e: 190 (16), 189 ($M^{\cdot+}$, 17), 173 (30), 172 (100), 157 (35), 144 (52), 143 (37), 131 (38), 130 (41), 129 (68), 128 (32), 117 (45), 115 (41), 109 (34), 108 (30), 107 (30), 106 (35), 105 (33), 94 (54), 92 (36), 91 (71), 80 (47), 79 (46), 77 (41). Anal. Calcd for $C_{13}H_{19}N \cdot HCl \cdot 0.33H_2O$ (231.77): C 67.37, H 8.99, N 6.04, Cl 15.30. Found: C 67.51, H 9.22, N 6.00, Cl 15.44.

***N*-Methyl[(pentacyclo[6.4.0.0^{2,10}.0^{3,7}.0^{4,9}]dodec-8-yl)methyl]-amine Hydrochloride (19·HCl).** To a stirred solution of **18**·HCl (225.8 mg, 1.0 mmol), Et_3N (0.55 mL, 3.76 mmol) in anhydrous Et_2O (10 mL) at 0 °C, methyl chloroformate (0.18 mL, 1.94 mmol) was added dropwise. When the addition was finished, the solution was stirred at room temperature for 18 h. Water (15 mL) was added, and the two layers were separated. The aqueous layer was extracted with EtOAc (3 × 10 mL). The combined organic extracts were washed with H_2O (1 × 10 mL), with 2 N HCl (2 × 10 mL), dried with anhydrous Na_2SO_4, filtered, and concentrated in vacuo to give the expected carbamate. This residue dissolved in anhydrous THF (2 mL) was added dropwise to a suspension of $LiAlH_4$ (265 mg, 7.0 mmol) in anhydrous THF (7 mL) at 0 °C. When the addition was finished, the suspension was heated under reflux for 20 h. The mixture was cooled to 0 °C (ice−water bath), treated with 5 N NaOH (3 mL), and stirred at room temperature for 1 h. The obtained solid was filtered through Celite in vacuo and washed with CH_2Cl_2 (3 × 10 mL). The filtrate was dried with anhydrous Na_2SO_4, filtered, treated with excess of HCl in Et_2O, and concentrated in vacuo to give the hydrochloride of **19**. Crystallization from MeOH/Et_2O gave pure **19**·HCl as a white solid (98.3 mg, 41% yield): mp >280 °C (dec.); IR (KBr) ν 3000−2750 (max at 2938, 2873, 2824, and 2754, N−H, $^+$N−H, and C−H st) cm^{-1}; ^{1}H NMR (500 MHz, CD_3OD) δ 1.15 [broad s, 1 H, 9-H], 1.48 × 1.67 [complex signal, 8 H, 5(11)-H$_\alpha$, 5(11)-H$_\beta$, 6(12)-H$_\alpha$ and 6(12)-H$_\beta$], 2.18 [broad s, 2 H, 4(10)-H], 2.21 [broad s, 2 H, 1(7)-H], 2.34 [d, J = 1.5 Hz, 2 H, 2(3)-H], 2.76 (s, 3 H, CH_3), 3.21 (s, 2 H, CH_2N), 4.85 (s, NH_2^+); ^{13}C NMR (100.6 MHz, CD_3OD) δ 23.1 [CH_2, C6(12)], 25.0 [CH_2, C5(11)], 34.9 (CH_3, CH_3NH), 48.9 (CH_2, CH_2N), 49.3 [CH, C2(3)], 50.8 (C, C8), 53.3 (CH, C9), 54.0 [CH, C4(10)], 54.3 [CH, C1(7)]. MS (EI), m/e (%): 203 ($M^{\bullet+}$, 15), 172 (100), 157 (44), 144 (52), 143 (38), 131 (26), 130 (30), 129 (49), 117 (25), 106 (31), 94 (59), 91 (48), 80 (69), 79 (33), 44 (81). Anal. Calcd for $C_{14}H_{21}N \cdot HCl$ (239.78): C 70.13, H 9.25, N 5.84, Cl 14.79. Found: C 70.37, H 9.30, N 5.81, Cl 14.91.

3-Azahexacyclo[7.6.0.0^{1,5}.0^{5,12}.0^{6,10}.0^{11,15}]pentadeca-7, 13-diene-1,2-dione (20). A mixture of diacid **12** (2.44 g, 10.0 mmol) and urea (3.00 g, 97% purity, 50.0 mmol) was heated slowly to 135 °C. When the mixture melted, it was heated to 180 °C for 30 min and cooled. Water (50 mL) was added, and the suspension was extracted with CH_2Cl_2 (6 × 30 mL). The combined organic extracts were washed with brine (1 × 45 mL), dried with anhydrous Na_2SO_4, filtered, and concentrated in vacuo to dryness to give imide **20** as a white solid (952 mg, 42% yield). An analytical sample of **20** was obtained by crystallization from CH_2Cl_2: mp >245 °C (dec); IR (KBr) ν 3187 (N−H), 1751 and 1718 (C═O st) cm^{-1}; ^{1}H NMR (500 MHz, $CDCl_3$) δ 2.87 [m, 2 H, 10(11)-H], 3.46 [m, 4 H, 6(9,12,15)-H], 6.07 [t, J = 2.0 Hz, 4 H, 7(8,13,14)-H], 7.96 (broad s, 1 H, NH); ^{13}C NMR (100.6 MHz, $CDCl_3$) δ 62.4 [CH, C6(9,12,15)], 64.4 [CH, C10(11)], 68.3 [C, C1(5)], 132.2 [CH, C7(8,13,14)], 175.5 (C, CO). MS (EI), m/e (%): 225 ($M^{\bullet+}$, 4), 160 (100), 153 (31), 152 (18). Anal. Calcd for $C_{14}H_{14}NO_2$ (225.24): C 74.65, H 4.92, N 6.22. Found: C 74.29, H 4.97, N 6.31.

3-Azahexacyclo[7.6.0.0^{1,5}.0^{5,12}.0^{6,10}.0^{11,15}]pentadeca-7, 13-diene Hydrochloride (21·HCl). To a stirred solution of imide **20** (1.45 g, 6.42 mmol) in anhydrous THF (50 mL) at 0 °C, $LiAlH_4$ (2.44 g, 64.2 mmol) was carefully added. When the addition was finished, the suspension was heated under reflux for 72 h. The mixture was cooled to 0 °C (ice−water bath), treated with 10 N NaOH till basic pH was obtained, and stirred at room temperature for 1 h. The obtained solid was filtered in vacuo through Celite and washed with CH_2Cl_2 (3 × 25 mL). The filtrate was dried with anhydrous Na_2SO_4, filtered, and evaporated in vacuo. The obtained solid residue was taken in Et_2O (20 mL) and treated with excess of HCl in Et_2O to give the hydrochloride of **21**. An analytical sample of **21**·HCl was obtained as a white solid by crystallization from MeOH/Et_2O: mp >240 °C (dec); IR (KBr) ν 3160, 3060, 2974, 2949, 2883, 2836, and 2736 (NH_2^+ st) cm^{-1}; ^{1}H NMR (500 MHz, DMSO-d_6) δ 2.77 (m, 2 H, 10(11)-H), 2.97 [s, 4 H, 2(4)-H$_2$], 3.11 [pseudo q, J = 2.5 Hz, 4 H, 6(9,12,15)-H], 4.86 (s, NH_2), 6.19 [t, J = 2.0 Hz, 4 H, 7(8,13,14)-H]; ^{13}C NMR (100.6 MHz, DMSO-d_6) δ 36.3 [CH_2, C2(4)], 53.3 [CH, C6(9,12,15)], 55.3 [CH, C10(11)],

63.3 [C, C1(5)], 125.4 [CH, C7(8,13,14)]. MS (EI), *m/e* (%): 197 ($M^{\bullet+}$, 55), 196 (35), 168 (24), 167 (26), 165 (27), 156 (30), 153 (25), 152 (30), 132 (64), 131 (91), 130 (100), 118 (48), 117 (38), 115 (51). Anal. Calcd for $C_{14}H_{15}N \cdot HCl$ (233.74): C 71.94, H 6.90, N 5.99, Cl 15.17. Found: C 71.80, H 7.08, N 5.91, Cl 15.47.

3-Azahexacyclo[7.6.0.0^{1,5}.0^{5,12}.0^{6,10}.0^{11,15}]pentadecane Hydrochloride (22·HCl). A suspension of **21**·HCl (150 mg, 0.64 mmol) and 5% Pd/C (50% in water, 10 mg) in absolute EtOH (20 mL) was hydrogenated at 1 atm for 48 h. The suspension was filtered. The residue was washed with EtOH, and the filtrate was concentrated in vacuo to give **22**·HCl as a white solid (150 mg, 99% yield). An analytical sample of **22**·HCl was obtained by crystallization from MeOH/Et_2O: mp >240 °C (dec.); IR (KBr) ν 2938, 2871, 2793, and 2765 (NH_2^+ st) cm^{-1}. ^{1}H NMR (500 MHz, CD_3OD) δ 1.62−1.68 [complex signal, 8 H, 7(8,13,14)-H$_\alpha$ and 7(8,13,14)-H$_\beta$], 2.24 [m, 4 H, 6(9,12,15)-H], 2.55 (broad s, 2 H, 10(11)-H), 3.11 [s, 4 H, 2(4)-H_2], 4.86 (s, NH_2); ^{13}C NMR (100.6 MHz, CD_3OD) δ 22.3 [CH_2, C7(8,13,14)], 41.5 [CH_2, C2(4)], 51.7 [CH, C10(11)], 56.1 [CH, C6(9,12,15)], 62.2 [C, C1(5)]. MS (EI), *m/e* (%): 201 ($M^{\cdot+}$, 100), 186 (23), 184 (36), 169 (50), 156 (27), 155 (27), 143 (32), 129 (45), 106 (70), 91 (50). Anal. Calcd for $C_{14}H_{19}N \cdot HCl \cdot 0.4H_2O$ (244.98): C 68.64, H 8.56, N 5.72, Cl 14.47. Found: C 68.59, H 8.56, N 5.56, Cl 14.41.

3-Azaoctacyclo[8.7.0.0^{1,5}.0^{5,13}.0^{6,11}.0^{7,9}.0^{12,17}.0^{14,16}]heptadecane-2,4-dione (23). To a suspension of imide **20** (2.50 g, 11.1 mmol) and $Pd(OAc)_2$ (62.8 mg, 0.28 mmol) in CH_2Cl_2 (5 mL) an ethereal solution of diazomethane (freshly prepared from *N*-methyl-*N*-nitrosourea, 10 g, 9.7 mmol) was added. The mixture was stirred at room temperature. Two further additions of ethereal solution of diazomethane were performed to achieve total conversion (^{1}H NMR control). The suspension was filtered. $NaHCO_3$ (saturated aqueous solution, 100 mL) was added, and the mixture was stirred at room temperature overnight. The organic layer was separated, dried with anhydrous Na_2SO_4, filtered, and evaporated in vacuo to give the imide **23** as a pale yellow solid (2.66 g, 95% yield). An analytical sample of **23** was obtained by crystallization from CH_2Cl_2/pentane: mp 277−278 °C (dec); IR (KBr) ν 3225 (NH st), 1751, 1721, and 1698 (C═O st) cm^{-1}. ^{1}H NMR (500 MHz, $CDCl_3$) δ 0.13 [dt, 2 H, J = 5.5 Hz, J' = 7.5 Hz, 8(15)-H$_{endo}$], 0.26 [dt, 2 H, J = 5.5 Hz, J' = 3.3 Hz, 8(15)-H$_{exo}$], 1.11 [dd, 4 H, J = 7.5 Hz, J' = 3.3 Hz, 7(9,14,16)-H], 1.93 [m, 2 H, 11(12)-H], 2.81 [dd, 4 H, J = 2.0 Hz, J' = 0.5 Hz, 6(10,13,17)-H], 8.28 (s, 1 H, NH); ^{13}C NMR (100.6 MHz, $CDCl_3$) δ 2.1 [CH_2, C8(15)], 9.6 [CH, C7(9,14,16)], 39.1 [CH, C11(12)], 55.2 [CH, C6(10,13,17)], 66.3 [C, C1(5)], 176.6 [C, C2(4)]. MS (EI), *m/e* (%): 253 ($M^{\cdot+}$, 21), 187 (24), 182 (20), 175 (31), 174 (26), 167 (32), 166 (23), 165 (48), 152 (27), 148 (30), 128 (28), 115 (38), 104 (25), 91 (38), 79 (100), 77 (61). Anal. Calcd For $C_{16}H_{15}NO_2$ (253.30): C 75.87, H 5.97, N 5.53. Found: C 75.64, H 5.77, N 5.49.

3-Azaoctacyclo[8.7.0.0^{1,5}.0^{5,13}.0^{6,11}.0^{7,9}.0^{12,17}.0^{14,16}]heptadecane Hydrochloride (24·HCl). To a stirred solution of imide **23** (763 mg, 3.01 mmol) in anhydrous THF (28 mL) at 0 °C, $LiAlH_4$ (1.14 g, 30.1 mmol) was carefully added. When the addition was finished, the suspension was heated under reflux for 72 h. The mixture was cooled to 0 °C (ice−water bath), treated with 10 N NaOH till basic pH was obtained, and stirred at room temperature for 1 h. The obtained solid was filtered in vacuo through Celite and was washed with CH_2Cl_2 (3 × 25 mL). The filtrate was dried with anhydrous Na_2SO_4, filtered, and evaporated in vacuo. The obtained solid residue was taken in EtOAc/Et_2O and treated with excess of HCl in Et_2O to give the hydrochloride of **24** as a solid (506 mg, 64% yield). An analytical sample of **24**·HCl was obtained by crystallization from CH_2Cl_2/pentane: mp 242−243 °C (dec); IR (KBr) ν 3446 (NH st) cm^{-1}. ^{1}H NMR (500 MHz, CD_3OD) δ 0.19 [dt, 2 H, J = 5.0 Hz, J' = 7.2 Hz, 8(15)-H$_{endo}$], 0.43 [dt, 2 H, J = 5.0 Hz, J' = 3.0 Hz, 8(15)-H$_{exo}$], 1.13 [dd, 4 H, J = 7.2 Hz, J' = 3.1 Hz, 7(9,14,16)-H], 1.89 [m, 2 H, 11(12)-H], 2.37 [broad s, 4 H, 6(10,13,17)-H], 3.29 [s, 4 H, 2(4)-H_2]; ^{13}C NMR (100.6 MHz, CD_3OD) δ 3.2 [CH_2, C8(15)], 10.3 [CH, C7(9,14,16)], 39.7 [CH, C11(12)], 41.9 [CH_2, C2(4)], 54.8 [CH, C6(10,13,17)], 66.5 [C, C1(5)]. MS (EI), *m/e* (%): 226 (19), 225 ($M^{\cdot+}$, 100), 224 (74), 170 (20), 165 (21), 146 (27), 145 (31), 144 (70), 132 (22), 130 (30), 129 (25), 128 (26), 118 (38), 117 (45), 115 (41), 91 (38), 80 (41), 79 (44), 77 (39). Anal. Calcd For $C_{16}H_{19}N \cdot HCl \cdot 1.25H_2O$ (284.31): C 67.59, H 7.98, N 4.93, Cl 12.47. Found: C 67.42, H 7.75, N 4.87, Cl 12.80.

Molecular Modeling. Docking studies and restrained molecular dynamics (MD) simulations were combined to explore the structural features of the binding of Amt and the ring-expanded compound **24** to the A/M2 ion channel. The PDB file 2kqt was used as template of the channel, as it provides the ssNMR structure of the M2TM region in DMPC bilayers bound to deuterated Amt.[15] Thus, it accounts for conformational changes in the transmembrane helices induced upon ligand binding. The structure of the channel was refined by energy minimization using AMBER[67] and the parmff99SB[68] force field by imposing suitable positional restraints to the backbone atoms (see below). The whole channel lumen was considered as the binding site in docking computations. The ligands were built up with MOE (Chemical Computing Group, Montreal, Canada). According to the expected basicity for primary and secondary amines at physiological pH, both Amt and **24** were modeled in the protonated form. The geometry was refined by energy minimization with the MMFF94 force field.[69] Docking simulations were carried out using rDock.[70,71] The best 50 poses for each ligand were considered to examine the binding of the compounds in the lumenal part of the channel.

Restrained molecular dynamics (MD) simulations were performed for three different models of Amt, which were built up by placing this compound with the amino group oriented toward the (i) C- and (ii) N-terminus of the pore and (iii) starting from the docked pose. Likewise, three distinct starting orientations were also considered for compound **24**: (i) the docking pose, (ii) by placing the main axis of the molecule aligned with the axis of the pore in the Amt binding site, and (iii) by placing **24** below the plane defined by Ala30, with the main axis normal to the pore axis and the amino group pointing toward the C-terminus (see Figure S4 in Supporting Information). Capping (acetyl, *N*-methyl) groups were added to the four helices in the ssNMR structure. TIP3P water molecules[72] were added to fill the lumenal region, paying particular attention to the positioning of the hydrating water molecules around the His37 box, as they have been recently identified in a X-ray structure of the channel (PDB entry 3LBW).[64] Correspondingly, only two His37 were protonated.[64] The geometries of Amt and **24**, both in their protonated state, were optimized at the B3LYP/6-31G(d) level, and partial charges were derived using the RESP procedure.[73] Standard atom types defined in the AMBER force field were assigned to the ligand.

The geometry of the system was minimized in four steps. First, the position of hydrogen atoms was optimized using 3000 steps of steepest descent algorithm. Then, water molecules were refined through 2000 steps of steepest descent followed by 3000 steps of conjugate gradient. Next, the position of the ligand and water molecules were optimized with 2000 steps of steepest descent and 4000 steps of conjugate gradient. Finally, the whole system was optimized with 3000 steps of steepest descent and 7000 steps of conjugate gradient. Thermalization of the system was performed in five steps of 100 ps, increasing the temperature from 50 to 298 K. A restraint of 25 kcal mol^{-1} Å^{-2} was applied through all the stages to the backbone atoms of the helices and to the side chains of His37 and Trp41. Then, a 250 ps MD simulation was run at 298 K, reducing progressively the restraint of the backbone atoms to 10 and 5 kcal mol^{-1} Å^{-2} for the heavy atoms in the side chain of Trp41. The addition of the restraints is necessary to preserve the global conformational state of the channel in the presence of bound ligand. Then, a series of restrained trajectories were run using a time step of 1 fs, SHAKE for those bonds containing hydrogen atoms, and a cutoff of 11 Å for

nonbonded interactions. In particular, three 40 ns MD simulations were run for Amt, each starting from one of the three different binding modes. For **24**, two trajectories were run for 40 ns (binding modes i and ii; see above), and in the third case (binding mode iii) the trajectory was continued up to 58 ns, when convergence in the binding mode of the ligand relative to the orientation adopted in the other two MD simulations was found (see Figure S5 in Supporting Information).

Finally, the solvent interaction energies (SIE) technique developed by Purisima and co-workers was used to estimate the interaction free energies for the different binding modes of Amt (see Table S1 in Supporting Information).[74,75]

■ ASSOCIATED CONTENT

Supporting Information. Figures S1−S5 (modeling studies) and S6 (CD titration assay), B3LYP/6-31G(d) optimized geometries of Amt and **24** and their RESP partial charges, and Table S1 listing solvent interaction energies (SIE). This material is available free of charge via the Internet at http://pubs.acs.org.

■ AUTHOR INFORMATION

Corresponding Author

*Phone: +34 934024533. Fax: +34 934035941. E-mail: svazquez@ub.edu.

■ ACKNOWLEDGMENT

M.D.D., E.T., S.V., J.J.-J., and F.J.L. thank the Spanish Ministerio de Ciencia e Innovación (FPU fellowship to MDD, PFIS fellowship to J.J.-J., Grants CTQ2008-03768 and SAF2008-0559) and the Generalitat de Catalunya (FI fellowship to E.T., Grant SCG-2009-294) for financial support. L.N. acknowledges financial support from the Fonds voor Wetenschappelijk Onderzoek Vlaanderen (FWO No. 9.0188.07) and the Geconcerteerde Onderzoeksacties (Grant GOA/10/014) and the technical assistance from L. Persoons and W. van Dam. The research was supported by NIH Research Grants R01 AI-57363 (L.H.P.) and U01 AI-1074571 (L.H.P., W.F.D., and R.A.L.).

■ ABBREVIATIONS USED

Amt, amantadine; BSA, bovine serum albumin; CD, circular dichroism; DMEM, Dulbecco's modified Eagle medium; DMPC, dimyristoylphosphatidylcholine; DPC, dodecylphosphocholine; MDCK, Madin−Darby canine kidney; MD, molecular dynamics; MTS, 3-(4,5-dimethylthiazol-2-yl)-5-(3-carboxymethoxyphenyl)-2-(4-sulfophenyl)-2*H*-tetrazolium; PBS, phosphate buffered saline; PDB, Protein Data Bank; ssNMR, solid state nuclear magnetic resonance; TEV, two-electrode voltage clamp; TM, transmembrane; wt, wild type

■ REFERENCES

(1) Lamb, R. A.; Holsinger, L. J.; Pinto, L. H. The Influenza A Virus M_2 Ion Channel Protein and Its Role in the Influenza Virus Life Cycle. In *Receptor-Mediated Virus Entry into Cells*; Wimmer, E., Ed.; Cold Spring Harbor Press: Cold Spring Harbor, NY, 1994; pp 303−321.

(2) Lamb, R. A.; Zebedee, S. L.; Richardson, C. D. Influenza virus M_2 protein is an integral membrane protein expressed on the infected-cell surface. *Cell* **1985**, *40*, 627–633.

(3) Skehel, J. J.; Wiley, D. C. Receptor binding and membrane fusion in virus entry: the influenza hemagglutinin. *Annu. Rev. Biochem.* **2000**, *69*, 531–569.

(4) Zhirnov, O. P. Solubilization of matrix protein M1/M from virions occurs at different pH for orthomyxo- and paramyxoviruses. *Virology* **1990**, *176*, 274–279.

(5) Grambas, S.; Hay, A. J. Maturation of influenza A virus hemagglutinin—estimates of the pH encountered during transport and its regulation by the M2 protein. *Virology* **1992**, *190*, 11–18.

(6) Hu, J.; Fu, R.; Nishimura, K.; Zhang, L.; Zhou, H.-X.; Busath, D. D.; Vijayvergiya, V.; Cross, T. A. Histidines, heart of the hydrogen ion channel from influenza A virus: toward an understanding of conductance and proton selectivity. *Proc. Natl. Acad. Sci. U.S.A.* **2006**, *103*, 6865–6870.

(7) Pinto, L. H. The M2 proton channels of influenza A and B viruses. *J. Biol. Chem.* **2006**, *281*, 8997–9000.

(8) Lagoja, I. M.; De Clercq, E. Anti-influenza virus agents: synthesis and mode of action. *Med. Res. Rev.* **2008**, *28*, 1–38.

(9) Tu, Q.; Pinto, L. H.; Luo, G.; Shaughnessy, M. A.; Mullaney, D.; Kurtz, S.; Krystal, M.; Lamb, R. A. Characterization of inhibition of M_2 ion channel activity by BL-1743, an inhibitor of influenza A virus. *J. Virol.* **1996**, *70*, 4246–4252.

(10) Wang, J.; Cady, S. D.; Balannik, V.; Pinto, L. H.; DeGrado, W. F.; Hong, M. Discovery of spiro-piperidine inhibitors and their modulation of the dynamics of the M2 proton channel from influenza A virus. *J. Am. Chem. Soc.* **2009**, *131*, 8066–8076.

(11) Bright, R. A.; Shay, D. K.; Shu, B.; Cox, N. J.; Klimov, A. I. Adamantane resistance among influenza A viruses isolated early during the 2005−2006 influenza season in the United States. *JAMA, J. Am. Med. Assoc.* **2006**, *295*, 891–894.

(12) Cady, S. D.; Mishanina, T. V.; Hong, M. Structure of amantadine-bound M2 transmembrane peptide of influenza A in lipid bilayers from magic-angle-spinning solid-state NMR: the role of Ser31 in amantadine binding. *J. Mol. Biol.* **2009**, *385*, 1127–1141.

(13) Cady, S. D.; Luo, W.; Hu, F.; Hong, M. Structure and function of the influenza A M2 proton channel. *Biochemistry* **2009**, *48*, 7356–7364.

(14) Deyde, V. M.; Xu, X.; Bright, R. A.; Shaw, M.; Smith, C. B.; Zhang, Y.; Shu, Y.; Gubareva, L. V.; Cox, N. J.; Klimov, A. I. Surveillance of resistance to adamantanes among influenza A(H3N2) and A(H1N1) viruses isolated worldwide. *J. Infect. Dis.* **2007**, *196*, 249–257.

(15) Cady, S. D.; Schmidt-Rohr, K.; Wang, J.; Soto, C. S.; Degrado, W. F.; Hong, M. Structure of the amantadine binding site of influenza M2 proton channels in lipid bilayers. *Nature* **2010**, *463*, 689–692.

(16) Chen, H.; Wu, Y.; Voth, G. A. Proton transport behavior through the influenza A M2 channel: insights from molecular simulation. *Biophys. J.* **2007**, *93*, 3470–3479.

(17) Duff, K. C.; Gilchrist, P. J.; Saxena, A. M.; Bradshaw, J. P. Neutron diffraction reveals the site of amantadine blockade in the influenza A M2 ion channel. *Virology* **1994**, *202*, 287–293.

(18) Jing, X.; Ma, C.; Ohigashi, Y.; Oliveira, F. A.; Jardetzky, T. S.; Pinto, L. H.; Lamb, R. A. Functional studies indicate amantadine binds to the pore of the influenza A virus M2 proton-selective ion channel. *Proc. Natl. Acad. Sci. U.S.A.* **2008**, *105*, 10967–10972.

(19) Khurana, E.; Dal Peraro, M.; DeVane, R.; Vemparala, S.; DeGrado, W. F.; Klein, M. L. Molecular dynamics calculations suggest a conduction mechanism for the M2 proton channel from influenza A virus. *Proc. Natl. Acad. Sci. U.S.A.* **2009**, *106*, 1069–1074.

(20) Stouffer, A. L.; Acharya, R.; Salom, D.; Levine, A. S.; Di Costanzo, L.; Soto, C. S.; Tereshko, V.; Nanda, V.; Stayrook, S.; DeGrado, W. F. Structural basis for the function and inhibition of an influenza virus proton channel. *Nature* **2008**, *451*, 596–599.

(21) Yi, M.; Cross, T. A.; Zhou, H. X. A secondary gate as a mechanism for inhibition of the M2 proton channel by amantadine. *J. Phys. Chem.* **2008**, *112*, 7977–7979.

(22) Schnell, J. R.; Chou, J. J. Structure and mechanism of the M2 proton channel of influenza A virus. *Nature* **2008**, *451*, 591–595.

(23) Ohigashi, Y.; Ma, C.; Jing, X.; Balannick, V.; Pinto, L. H.; Lamb, R. A. An amantadine-sensitive chimeric BM2 ion channel of influenza B virus has implications for the mechanism of drug inhibition. *Proc. Natl. Acad. Sci. U.S.A.* **2009**, *106*, 18775–18779.

(24) Balannik, V.; Wang, J.; Ohigashi, Y.; Jing, X.; Magavern, E.; Lamb, R. A.; DeGrado, W. F.; Pinto, L. H. Design and pharmacological characterization of inhibitors of amantadine-resistant mutants of the M2 ion channel of influenza A virus. *Biochemistry* **2009**, *48*, 11872–11882.

(25) Balannik, V.; Carnevale, V.; Fiorin, G.; Levine, B. G.; Lamb, R. A.; Klein, M. L.; DeGrado, W. F.; Pinto, L. H. Functional studies and modeling of pore-lining residue mutants of the influenza a virus M2 ion channel. *Biochemistry* **2010**, *49*, 696–708.

(26) Rosenberg, M. R.; Casarotto, M. G. Coexistence of two adamantane binding sites in the influenza A M2 ion channel. *Proc. Natl. Acad. Sci. U.S.A.* **2010**, *107*, 13866–13871.

(27) Bright, R. A.; Medina, M. J.; Xu, X.; Pérez-Oronoz, G.; Wallis, T. R.; Davis, X. M.; Povinelli, L.; Cox, N. J.; Klimov, A. I. Incidence of adamantane resistance among influenza A (H3N2) viruses isolated worldwide from 1994 to 2005: a cause for concern. *Lancet* **2005**, *366*, 1175–1181.

(28) Saito, R.; Sakai, T.; Sato, I.; Sano, Y.; Oshitani, H.; Sato, M.; Suzuki, H. Frequency of amantadine-resistant influenza A viruses during two seasons featuring cocirculation of H1N1 and H3N2. *J. Clin. Microbiol.* **2003**, *41*, 2164–2165.

(29) Hien, T. T.; Boni, M. F.; Bryant, J. E.; Ngan, T. T.; Wolbers, M.; Nguyen, T. D.; Truong, N. T.; Dung, N. T.; Ha do, Q.; Hien, V. M.; Thanh, T. T.; Nhu le, N. T.; Uyen le, T. T.; Nhien, P. T.; Chinh, N. T.; Chau, N. V.; Farrar, J.; van Doorn, H. R. Early pandemic influenza (2009 H1N1) in Ho Chi Minh City, Vietnam: a clinical virological and epidemiological analysis. *PLoS Med.* **2010**, *7*, No. e1000277.

(30) Pebody, R.; McLean, E.; Zhao, H.; Cleary, P.; Bracebridge, S.; Foster, K.; Charlett, A.; Hardelid, P.; Waight, P.; Ellis, J.; Bermingham, A.; Zambon, M.; Evans, B.; Salmon, R.; McMenamin, J.; Smyth, B.; Catchpole, M.; Watson, J. Pandemic influenza A (H1N1) 2009 and mortality in the United Kingdom: risk factors for death, April 2009 to March 2010. *Eurosurveillance* **2010**, *15* (20).

(31) Geluk, H. W.; Schut, J.; Schlatmann, J. L. M. A. Synthesis and antiviral properties of 1-adamantylguanidine. A modified method for preparing *t*-alkylguanidines. *J. Med. Chem.* **1969**, *12*, 712–715.

(32) Aldrich, P. E.; Hermann, E. C.; Meier, W. E.; Paulshock, M.; Prichard, W. W.; Snyder, J. A.; Watts, J. C. Antiviral agents. 2. Structure—activity relationships of compounds related to 1-adamantanamine. *J. Med. Chem.* **1971**, *14*, 535–543.

(33) Lundahl, K.; Schut, J.; Schlatmann, J. L. M. A.; Paerels, G. B.; Peters, A. Synthesis and antiviral activities of adamantane spiro compounds. 1. Adamantane and analogous spiro-3′-pyrrolidines. *J. Med. Chem.* **1972**, *15*, 129–132.

(34) Van Hes, R.; Smit, A.; Kralt, T.; Peters, A. Synthesis and antiviral activities of adamantane spiro compounds. 2. *J. Med. Chem.* **1972**, *15*, 132–136.

(35) Mathur, A.; Beare, A. S.; Reed, S. E. In vitro antiviral activity and preliminary clinical trials of a new adamantane compound. *Antimicrob. Agents Chemother.* **1973**, *4*, 421–426.

(36) Aigami, K.; Inamoto, Y.; Takaishi, N.; Hattori, K.; Takatsuki, A.; Tamura, G. Biologically active polycycloalkanes. 1. Antiviral adamantane derivatives. *J. Med. Chem.* **1975**, *18*, 713–721.

(37) Kolocouris, N.; Foscolos, G. B.; Kolocouris, A.; Marakos, P.; Pouli, N.; Fytas, G.; Ikeda, S.; De Clercq, E. Synthesis and antiviral activity of some aminoadamantane derivatives. *J. Med. Chem.* **1994**, *37*, 2896–2902.

(38) Kolocouris, N.; Kolocouris, A.; Foscolos, G. B.; Fytas, G.; Neyts, J.; Padalko, E.; Balzarini, J.; Snoeck, R.; Andrei, G.; De Clercq, E. Synthesis and antiviral activity of some new aminoadamantane derivatives. 2. *J. Med. Chem.* **1994**, *37*, 2896–2902.

(39) Scholtissek, C.; Quack, G.; Klenk, H. D.; Webster, R. G. How to overcome resistance of influenza A viruses against adamantane derivatives. *Antiviral Res.* **1998**, *37*, 83–95.

(40) Stamatiou, G.; Foscolos, G. B.; Futas, G.; Kolocouris, A.; Kolocouris, N.; Pannecouque, C.; Witvrouw, M.; Padalko, E.; Neyts, J.; De Clercq, E. Heterocyclic rimantadine analogues with antiviral activity. *Bioorg. Med. Chem.* **2003**, *11*, 5485–5492.

(41) Stylianakais, I.; Kolocouris, A.; Kolocouris, N.; Fytas, G.; Foscolos, G. B.; Padalko, E.; Neyts, J.; De Clercq, E. Spiro[pyrrolidine-2,2′-adamantanes]: synthesis, anti-influenza virus activity and conformational properties. *Bioorg. Med. Chem. Lett.* **2003**, *13*, 1699–1703.

(42) Zoidis, G.; Kolocouris, N.; Foscolos, G. B.; Kolocouris, A.; Fytas, G.; Karayannis, P.; Padalko, E.; Neyts, J.; De Clercq, E. Are the 2-isomers of the drug rimantadine active anti-influenza A agents?. *Antiviral Chem. Chemother.* **2003**, *14*, 153–164.

(43) Setaki, D.; Tataridis, D.; Stamatiou, G.; Kolocouris, A.; Foscolos, G. B.; Fytas, G.; Kolocouris, N.; Padalko, E.; Neyts, J.; De Clercq, E. Synthesis, conformational characteristics and anti-influenza virus A activity of some 2-adamantylsubstituted azacycles. *Bioorg. Chem.* **2006**, *34*, 248–273.

(44) Zoidis, G.; Fytas, C.; Papanastasiou, I.; Foscolos, G. B.; Fytas, G.; Padalko, E.; De Clercq, E.; Naesens, L.; Neyts, J.; Kolocouris, N. Heterocyclic rimantadine analogues with antiviral activity. *Bioorg. Med. Chem.* **2006**, *14*, 3341–3348.

(45) Tataridis, D.; Fytas, G.; Kolocouris, A.; Fytas, C.; Kolocouris, N.; Foscolos, G. B.; Padalko, E.; Neyts, J.; De Clercq, E. Influence of an additional 2-amino substituent of the 1-aminoethyl pharmacophore group on the potency of rimantadine against influenza virus A. *Bioorg. Med. Chem. Lett.* **2007**, *17*, 692–696.

(46) Kolocouris, N.; Zoidis, G.; Foscolos, G. B.; Fytas, G.; Prathalingham, S. R.; Kelly, J. M.; De Clercq, E. Design and synthesis of bioactive adamantane spiro heterocycles. *Bioorg. Med. Chem. Lett.* **2007**, *17*, 4358–4362.

(47) Zoidis, G.; Tsotinis, A.; Kolocouris, N.; Kelly, J. M.; Prathalingham, S. R.; Naesens, L.; De Clercq, E. Design and synthesis of bioactive 1,2-annulated adamantane derivatives. *Org. Biomol. Chem.* **2008**, *6*, 3177–3185.

(48) Kolocouris, A.; Spearpoint, P.; Martin, S. R.; Hay, A. J.; López-Querol, M.; Sureda, F. X.; Padalko, E.; Neyts, J.; De Clercq, E. Comparisons of the influenza virus A M2 channel binding affinities, anti-influenza virus potencies and NMDA antagonistic activities of 2-alkyl-2-aminoadamantanes and analogues. *Bioorg. Med. Chem. Lett.* **2008**, *18*, 6156–6160.

(49) Zoidis, G.; Kolocouris, N.; Naesens, L.; De Clercq, E. Design and synthesis of 1,2-annulated adamantane piperidines with anti-influenza virus activity. *Bioorg. Med. Chem.* **2009**, *17*, 1534–1541.

(50) Zarubaev, V. V.; Golod, E. L.; Anfimov, P. M.; Shtro, A. A.; Saraev, V. V.; Gavrilov, A. S.; Logvinov, A. V.; Kiselev, O. I. Synthesis and anti-viral activity of azolo-adamantanes against influenza A virus. *Bioorg. Med. Chem.* **2010**, *18*, 839–848.

(51) Whitney, J. G.; Gregory, W. A.; Kauer, J. C.; Roland, J. R.; Snyder, J. A.; Benson, R. E.; Hermann, E. C. Antiviral agents. I. Bicyclo[2.2.2]octan- and -oct-2-enamines. *J. Med. Chem.* **1970**, *13*, 254–260.

(52) Aigami, K.; Inamoto, Y.; Takaishi, N.; Hattori, K.; Takatsuki, A.; Tamura, G. Biologically active polycycloalkanes. 1. Antiviral adamantane derivatives. *J. Med. Chem.* **1975**, *18*, 713–721.

(53) Inamoto, Y.; Aigami, K.; Takaishi, N.; Fujikura, Y.; Ohsugi, M.; Ikeda, H.; Tsuchihashi, K. Biologically active polycycloalkanes. 6. Antiviral 1-tricyclo[4.3.1.$1^{2,5}$]undecyl derivatives. *J. Med. Chem.* **1979**, *22*, 1206–1214.

(54) Al-Nakib, W.; Higgins, P. G.; Willman, J.; Tyrrell, D. A. J.; Swallow, D. L.; Hurst, B. C.; Rushton, A. Prevention and treatment of experimental influenza A virus infection in volunteers with a new antiviral ICI 130685. *J. Antimicrob. Chemother.* **1986**, *18*, 119–129.

(55) García, A.; Teso, E.; García, A.; de la Moya, S.; Rodríguez, M. E.; Martínez, P.; Subramanian, L. R.; García, A. Synthesis of substituted 1-norbornylamines with antiviral activity. *J. Med. Chem.* **1995**, *38*, 4474–4477.

(56) Hu, W.; Zeng, S.; Li, C.; Jie, Y.; Li, Z.; Chen, L. Identification of hits as matrix-2 protein inhibitors through the focused screening of a small primary amine library. *J. Med. Chem.* **2010**, *53*, 3831–3834.

(57) Camps, P.; Duque, M. D.; Vázquez, S.; Naesens, L.; De Clercq, E.; Sureda, F. S.; López-Querol, M.; Camins, A.; Pallàs, M.; Prathalingam, S. R.; Kelly, J. M.; Romero, V.; Ivorra, D.; Cortés, D. Synthesis and pharmacological evaluation of several ring-contracted amantadine analogs. *Bioorg. Med. Chem.* **2008**, *16*, 9925–9936.

(58) Duque, M. D.; Camps, P.; Profire, L.; Montaner, S.; Vázquez, S.; Sureda, F. S.; Mallol, J.; López-Querol, M.; Naesens, L.; De Clercq, E.; Prathalingam, S. R.; Kelly, J. M. Synthesis and pharmacological evaluation of (2-oxaadamant-1-yl)amines. *Bioorg. Med. Chem.* **2009**, *17*, 3198–3206.

(59) Paquette, L. A. Dodecahedranes and allied spherical molecules. *Chem. Rev.* **1989**, *89*, 1051–1065.

(60) McNeil, D.; Vogt, B. R.; Sudol, J. J.; Theodoropulos, S.; Hedaya, E. Multiple cycloaddition reaction of 9,10-dihydrofulvalene. New approach to 3,4,7-methenocyclopenta[*a*]pentalene derivatives. *J. Am. Chem. Soc.* **1974**, *96*, 4673–4674.

(61) Taylor, R. T.; Pelter, M. W.; Paquette, L. A. Domino Diels−Alder reaction: 3,3a,3b,4,6a,7a-hexahydro-3,4,7-metheno-7*H*-cyclopenta[*a*]pentalene-7,8-dicarboxylic acid. *Org. Synth.* **1990**, *68*, 198–205.

(62) Camps, P.; Lukach, A. E.; Rossi, R. A. Synthesis of several halobisnoradamantane derivatives and their reactivity through the $S_{RN}1$ mechanism. *J. Org. Chem.* **2001**, *66*, 5366–5373.

(63) Khurana, E.; DeVane, R. H.; Dal Peraro, M.; Klein, M. L. Computational study of drug binding to the membrane-bound tetrameric M2 peptide bundle from influenza A virus. *Biochim. Biophys. Acta* **2011**, *1808*, 530–537.

(64) Acharya, R.; Carnevale, V.; Fiorin, G.; Levine, B. G.; Polischuk, A. L.; Balannik, V.; Samish, I.; Lamb, R. A.; Pinto, L. H.; DeGrado, W. F.; Klein, M. L. Structure and mechanism of proton transport through the transmembrane tetrameric M2 protein bundle of the influenza A virus. *Proc. Natl. Acad. Sci. U.S.A.* **2010**, *107*, 15075–15080.

(65) Ma, C.; Soto, C. S.; Ohigashi, Y.; Taylor, A.; Bournas, V.; Glawe, B.; Udo, M. K.; DeGrado, W. F.; Lamb, R. A.; Pinto, L. H. Identification of the pore-lining residues of the BM2 ion channel protein of influenza B virus. *J. Biol. Chem.* **2008**, *283*, 15921–15931.

(66) Vanderlinden, E.; Göktas, F.; Cesur, Z.; Froeyen, M.; Reed, M. L.; Russell, C. J.; Cesur, N.; Naesens, L. Novel inhibitors of influenza virus fusion: structure-activity relationship and interaction with the viral hemagglutinin. *J. Virol.* **2010**, *84*, 4277–4288.

(67) Case, D. A.; Darden, T. A.; Cheatham, T. E., III; Simmerling, C. L.; Wang, J.; Duke, R. E.; Luo, R.; Merz, K. M.; Pearlman, D. A.; Crowley, M.; Walker, R. C.; Zhang, W.; Wang, B.; Hayik, S; Roitberg, A.; Seabra, G.; Wong, K. F.; Paesani, F.; Wu, X.; Brozell, S.; Tsui, V.; Gohlke, H.; Yang, L.; Tan, C.; Mongan, J.; Hornak, V.; Cui, G.; Beroza, P.; Mathews, D. H.; Schafmeister, C.; Ross, W. S.; Kollman, P. A. *AMBER*, version 9; University of California: San Francisco, CA, 2006.

(68) Hornak, V.; Abel, R.; Okur, A.; Strockbine, B.; Roitberg, A.; Simmerling, C. Comparison of multiple Amber force fields and development of improved protein backbone parameters. *Proteins: Struct., Funct., Bioinf.* **2006**, *65*, 712–725.

(69) Halgren, T. A.; MMFF, V. I. MMFF94s option for energy minimization studies. *J. Comput. Chem.* **1999**, *20*, 720–729.

(70) Morley, S. D.; Afshar, M. Validation of an empirical RNA-ligand scoring function for fast flexible docking using RiboDock. *J.Comput.-Aided Mol. Des.* **2004**, *18*, 189–208.

(71) Barril, X.; Hubbard, R. E.; Morley, S. D. Virtual screening in structure-based drug discovery. *Mini-Rev. Med. Chem.* **2004**, *4*, 779–791.

(72) Jorgensen, W. L.; Chandrasekhar, J.; Madura, J. D.; Impey, R. W.; Klein, M. L. Comparison of simple potential functions for simulating liquid water. *J. Chem. Phys.* **1983**, *79*, 926–935.

(73) Bayly, C. I.; Cieplak, P.; Cornell, W.; Kollman, P. A. A well-behaved electrostatic potential based method using charge restraints for deriving atomic charges: the RESP model. *J. Phys. Chem.* **1993**, *97*, 10269–10280.

(74) Naïm, M.; Bhat, S.; Rankin, K. N.; Dennis, S.; Chowdhury, S. F.; Siddiqi, I.; Drabik, P.; Sulea, T.; Bayly, C. I.; Jakalian, A.; Purisima, E. O. Solvated interaction energy (SIE) for scoring protein−ligand binding affinities. 1. Exploring the parameter space. *J. Chem. Inf. Model.* **2007**, *47*, 122–133.

(75) Cui, Q.; Sulea, T.; Schrag, J. D.; Munger, C.; Hung, M.-N.; Nam, M.; Cygler, M.; Purisima, E. O. Molecular dynamics-solvated interaction energy studies of protein−protein interactions: the MP1-p14 scaffolding complex. *J. Mol. Biol.* **2008**, *379*, 787–802.